273

Anisotropic rotational diffusion of perdeuterated HIV protease from ^{15}N NMR relaxation measurements at two magnetic fields

Nico Tjandra[a], Paul Wingfield[b], Stephen Stahl[b] and Ad Bax[a]

[a]*Laboratory of Chemical Physics, National Institutes of Diabetes and Digestive and Kidney Diseases,
National Institutes of Health, Bethesda, MD 20892-0520, U.S.A.*
[b]*Protein Expression Laboratory, National Institute of Arthritis and Muscoskeletal and Skin Diseases,
National Institutes of Health, Bethesda, MD 20892, U.S.A.*

Summary

^{15}N NMR relaxation times in perdeuterated HIV-1 protease, complexed with the sub-nanomolar inhibitor DMP323, have been measured at 600 and 360 MHz ^{1}H frequency. The relative magnitudes of the principal components of the inertia tensor, calculated from the X-ray coordinates of the protein–drug complex, are 1.0:0.85:0.44. The relation between the T_1/T_2 ratios observed for the individual backbone amides and their N-H orientation within the 3D structure of the protease dimer yields a rotational diffusion tensor oriented nearly collinear to the inertia tensor. The relative magnitudes of its principal components (1.00:1.11:1.42) are also in good agreement with hydrodynamic modeling results. The orientation and magnitude of the diffusion tensors derived from relaxation data obtained at 360 and 600 MHz are nearly identical. The anisotropic nature of the rotational diffusion has little influence on the order parameters derived from the ^{15}N T_1 and T_2 relaxation times; however, if anisotropy is ignored, this can result in erroneous identification of either exchange broadening or internal motions on a nanosecond time scale. The average ratio of the T_1 values measured at 360 and 600 MHz is 0.50 ± 0.015, which is slightly larger than the value of 0.466 expected for an isotropic rigid rotor with $\tau_c = 10.7$ ns. The average ratio of the T_2 values measured at 360 and 600 MHz is 1.14 ± 0.04, which is also slightly larger than the expected ratio of 1.11. This magnetic field dependence of the T_1 and T_2 relaxation times suggests that the spectral density contribution from fast internal motions is not negligible, and that the chemical shift anisotropy of peptide backbone amides, on average, is larger than the 160 ppm value commonly used in ^{15}N relaxation studies of proteins.

Introduction

^{15}N and ^{13}C NMR relaxation times have been widely used to probe the internal dynamics of proteins (Allerhand et al., 1971; King et al., 1978; Wüthrich and Wagner, 1978; London, 1980; Lipari and Szabo, 1982a,b; Nirmala and Wagner, 1988; Dellwo and Wand, 1989; Kay et al., 1989; Boyd et al., 1990; Clore et al., 1990a,b; Kördel et

al., 1992; Peng and Wagner, 1992; Schneider et al., 1992; Palmer III, 1993; Torchia et al., 1993; Wagner, 1993). When relaxation data is obtained for a sufficient number of sites in the protein and the structure of the protein is known, such studies also provide information on the rotational diffusion tensor. This latter information can be particularly useful for the study of multi-domain proteins, where the rotational diffusion tensors of the individual

---

domains can provide important structural information related to their relative mobility (Barbato et al., 1992; Hansen et al., 1994; Brüschweiler et al., 1995; Tjandra et al., 1995a,b).

Although isotropic rotational diffusion is assumed in most NMR studies of internal protein dynamics, such an assumption is justified only when the deviations of ^{15}N (or ^{13}C) T_1/T_2 ratios from their average ratio do not exceed the individual experimental uncertainties. It is also commonly assumed that T_1/T_2 ratios are, to first order, not influenced by very rapid internal dynamics. This paper demonstrates that these assumptions are no longer strictly valid when data are acquired at high precision. Also, it is well recognized that conformational exchange processes that take place on a microsecond or millisecond time scale can shorten the transverse relaxation time and thereby increase the T_1/T_2 ratio. As a result, it can be difficult to separate the effects of such slow internal motions from the effects of anisotropic rotational diffusion (Schurr et al., 1994). However, if the relative orientations of the ^{15}N-^1H or ^{13}C-^1H bond vectors are known, one can simply test whether the T_1/T_2 ratios measured for the individual atoms correlate with the orientation of the bond vectors in a statistically significant manner. Using such a procedure, we recently have shown that the rotational diffusion of human ubiquitin is described by an axially symmetric diffusion tensor with an anisotropy, $D_\parallel/D_\perp$, of 1.17 (Tjandra et al., 1995b). The principal components of the ubiquitin inertia tensor, calculated from the X-ray coordinates, have relative ratios of 1.00:0.90:0.64, and the axis with the smallest moment of inertia was found to nearly coincide with the unique axis of the diffusion tensor. A detailed analysis showed that the fit between experimental and predicted T_1/T_2 ratios, when using a fully asymmetric diffusion tensor, did not yield a statistically significant improvement over the fit to an axially symmetric tensor.

The present study applies similar methodology to investigate the rotational dynamics of the HIV-1 protease homodimer, complexed with the inhibitor DMP323 (k_D = 0.25 nM) (Lam et al., 1994). The dimer consists of two times 99 residues and binds one C_2-symmetric inhibitor molecule in its active site. The total molecular mass of the complex is 22 kDa. The inertia tensor, calculated from the X-ray coordinates (Lam et al., 1994), has relative ratios of 1.0:0.85:0.44 for its principal components, and the principal axis with the intermediate moment of inertia coincides with the C_2 symmetry axis of the complex. As will be shown below, analysis of the relaxation data indicates that the rotational diffusion is best described by a fully asymmetric tensor. This represents the first case where a fully asymmetric rotational diffusion tensor is characterized experimentally by NMR relaxation data. NMR experiments are conducted at two magnetic fields, corresponding to ^1H frequencies of 360 and 600 MHz. It

will be shown that the diffusion tensors derived from the two data sets are in excellent agreement with one another.

The increase in ^{15}N T_1 with increasing magnetic field is found to be slightly smaller than predicted, assuming a chemical shift anisotropy (CSA) of 160 ppm. Similarly, the decrease in T_2 with increasing magnetic field is slightly larger than expected. A similar discrepancy between predicted and observed magnetic field dependence of the relaxation rates was noted recently by Peng and Wagner (1995). Here we propose that this difference between predicted and observed magnetic field dependence largely can be explained by a ^{15}N CSA which is, on average, about 10 ppm larger than the commonly used value of 160 ppm.

The present study is carried out on a protein where the non-exchangeable hydrogens are more than 85% deuterated, and represents the first time that detailed ^{15}N relaxation data are reported for a perdeuterated protein. Perdeuteration is found to increase the spectral quality of the ^1H-^{15}N correlation map, but no systematic changes relative to a previous relaxation study of the same protonated complex were found (Nicholson et al., 1995). This previous ^{15}N NMR study assumed isotropic rotational diffusion of the protease–inhibitor complex. Although the present study indicates that this assumption was not valid, we will show that the order parameters remain virtually unchanged relative to those reported in the earlier study, provided they are not simply derived from the spectral density at zero frequency.

Materials and Methods

The NMR sample of ^{15}N-enriched protease–DMP323 complex was prepared as described previously (Nicholson et al., 1995), except that the bacterial growth medium contained 99% D_2O, resulting in a protein with ≥ 85% deuteration of its non-exchangeable protons. The amino acid sequence of the protease used in the present study is PQVTLWQRPL VTIKIGGQLK EALLDTGADD TV-LEEMSLGR WKKMIGGI GGFIKVRQYD QILIEI-AGHK AIGTVLVGPT PVNIIGRNLL TQIGATLNF, which includes a C67A mutation relative to the protease–DMP323 complex from which the X-ray structure was obtained. Considering that the ^{15}N-^1H HSQC spectrum for the mutant is identical to that obtained previously for the protonated sample of the same protease (data not shown), perdeuteration of the protein does not affect its structure. With the exception of residue 67, the ^{15}N-^1H HSQC spectrum of the mutant used in this study and the protein used in the crystal structure are virtually the same, indicating that their structures are also very similar.

Deuteration of the non-exchangeable protons narrows the ^1H line width considerably, as seen in a 2D ^1H-^{15}N HSQC spectrum, and thereby reduces spectral overlap,
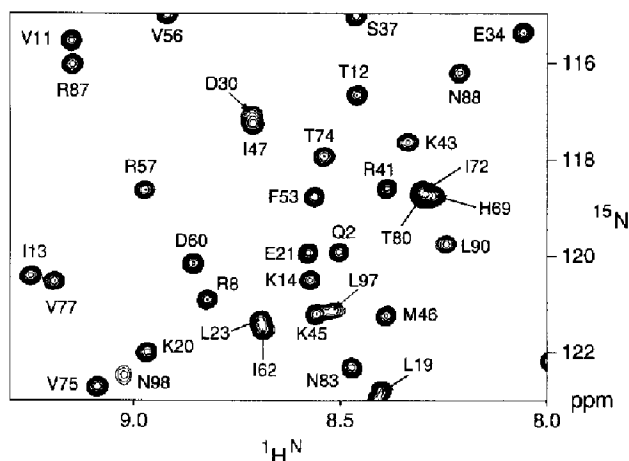
Fig. 1. Small region of the 360 MHz ^{1}H-^{15}N correlation spectrum of perdeuterated HIV-1 protease, complexed with DMP323, dissolved in 95% H_2O/5% D_2O. The spectrum corresponds to the first time point of a set of eight such spectra, recorded for measuring the ^{15}N T_1.

particularly in spectra recorded at 360 MHz ^{1}H frequency. Unfortunately, the corresponding improvement in sensitivity is largely offset by the longer T_1 of the amide protons ($\sim 4.8 \pm 0.5$ s at 600 MHz) compared to the fully protonated sample (~ 1.5 s). The NMR sample (250 µl in a Shigemi microcell) contained 0.75 mM of the protease dimer in H_2O/D_2O (95%/5%), and 50 mM sodium acetate buffer (pH 5.2). Experiments were carried out at 27 °C on Bruker AMX-360 and AMX-600 spectrometers, both equipped with inverse probeheads containing self-shielded z-gradients.

The T_1 relaxation decay was sampled at eight different time points (8, 16, 48, 120, 288, 544, 864 and 1184 ms at 600 MHz; 8, 40, 96, 160, 256, 416, 592 and 768 ms at 360 MHz) and the $T_{1\rho}$ decay curve was sampled at 10, 18, 26, 38, 56, 74, 110 and 146 ms, at both field strengths, using a ^{15}N spin-lock field strength of 2.5 kHz in both cases. $T_{1\rho}$ data were corrected for resonance offset effects as described in Results and Discussion. The total data collection time for each series of eight T_1 and $T_{1\rho}$ spectra was ~14 h at 600 MHz and ~23 h at 360 MHz. In order to minimize the effects of spectrometer drift during the lengthy experiment, all data were acquired in an interleaved manner, i.e., data were acquired for all eight time points before t_1 incrementation.

The ^{15}N-{^{1}H} NOE was measured using the water-flipback NOE method (Grzesiek and Bax, 1993) and was also recorded in an interleaved manner, analogous to the T_1 and T_2 measurements. Correcting the NOE data for the finite delay (9.6 s) between scans (Grzesiek and Bax, 1993) decreased NOE values by a few percent relative to the intensity ratios in two spectra recorded with and without saturation of the ^{1}H spectrum.

The relaxation data are shown in Fig. 2 and are available as supplementary material. The T_1 and T_2 data represent the averaged values from two separate measurements,

conducted several weeks apart. The pairwise root-mean-square differences (rmsd) between the two measurements were 22 ms (600 MHz, T_1), 4.6 ms (600 MHz, $T_{1\rho}$), 13.5 ms (360 MHz, T_1), and 4.6 ms (360 MHz, $T_{1\rho}$). The random errors in the averaged values are twofold smaller than the pairwise rmsd. The uncertainty in the ^{15}N-{^{1}H} NOE, measured at 600 MHz ^{1}H frequency, is estimated to be ± 0.025 on the basis of the rms noise in the reference and attenuated NOE spectra.

Results and Discussion

Relation between diffusion and relaxation rates

The relaxation times are related to the spectral density function, $J(\omega)$, according to:

$$1/T_1 = d^2 [J(\omega_N - \omega_H) + 3J(\omega_N) + 6J(\omega_N + \omega_H)] + c^2 J(\omega_N) \tag{1a}$$

$$1/T_2 = (1/2)d^2 [4J(0) + J(\omega_N - \omega_H) + 3J(\omega_N) + 6J(\omega_H) + 6J(\omega_N + \omega_H)] + (1/6)c^2 [4J(0) + 3J(\omega_N)] \tag{1b}$$

$$NOE = 1 + (\gamma_H/\gamma_N) d^2 [6J(\omega_N + \omega_H) - J(\omega_N - \omega_H)] \times T_1 \tag{1c}$$

where $d^2 = (1/10)[\gamma_N \gamma_H h/(2\pi \langle r_{HN}^3 \rangle)]^2$ and $c^2 = (2/15)[\omega_N(\sigma_\parallel - \sigma_\perp)]^2$, γ_N and γ_H are the ^{15}N and ^{1}H gyromagnetic ratios and ω_N and ω_H are the corresponding angular resonance frequencies, h is Planck's constant, r_{HN} is the internuclear distance, assumed to be 1.02 Å, and $\sigma_\parallel - \sigma_\perp$ is the ^{15}N chemical shielding anisotropy (opposite sign relative to CSA), commonly assumed to be -160 ppm. The spectral density function, $J(\omega)$, is defined as the Fourier transform of the correlation function, $C(t)$:

$$J(\omega) = \int_0^\infty C(t) \cos(\omega t) \, dt \tag{2a}$$

where $C(t) = \langle P_2(\mu(0) \cdot \mu(t)) \rangle$, and $P_2(x) = (3x^2 - 1)/2$. This definition of $J(\omega)$ differs by a factor 2/5 from the one used by others, reflecting the different normalization of the correlation function ($C(0) = 1$ in our case) and the different integral limits (0 to ∞ instead of $-\infty$ to $+\infty$). Correspondingly, the constants d^2 and c^2 in Eq. 1 are 5/2 times smaller than analogous constants used by others. For the case of anisotropic diffusion, the spectral density function is given by (Woessner, 1962; Lipari and Szabo, 1982a):

$$J(\omega) = S^2 \sum_{k=1,...5} A_k[\tau_k/(1 + \omega^2 \tau_k^2)] + (1 - S^2)[\tau/(1 + \omega^2 \tau^2)] \tag{2b}$$

with $A_1 = 6m^2 n^2$, $A_2 = 6p^2 n^2$, $A_3 = 6p^2 m^2$, $A_4 = d-e$, $A_5 = d+e$, where $d = [(3(p^4+m^4+n^4)-1]/2$, $e = [\delta_x(3p^4+6m^2n^2-1) + \delta_y(3m^4+$

$6p^2n^2-1)+\delta_x(3n^4+6p^2m^2-1)]/6$, and $\delta_i=(D_i-D)/(D^2-L^2)^{1/2}$. D is defined as 1/3 the trace of the diffusion tensor, $D = 1/3(D_x+D_y+D_z)$, and $L^2=1/3(D_xD_y+D_xD_z+D_yD_z)$. The corresponding time constants are defined as follows: $\tau_1=(4D_x + D_y+D_z)^{-1}$, $\tau_2=(4D_y+D_x+D_z)^{-1}$, $\tau_3=(4D_z+D_x+D_y)^{-1}$, $\tau_4 = [6(D+(D^2-L^2)^{1/2})]^{-1}$, and $\tau_5=[6(D-(D^2-L^2)^{1/2})]^{-1}$. The direction cosines of the N-H vector, p, m, and n, are defined relative to the principal axes, x, y, and z, respectively, of the diffusion tensor. The generalized order parameter S^2 describes the effect of internal motions occurring on a time scale τ_e, which are assumed to be fast compared to rotational diffusion. The approximation $\tau^{-1}=6D+\tau_e^{-1}$ is made to ensure compatibility with the model-free spectral density functions applicable to the isotropic case (Tjandra et al., 1995b).

Measurement of relaxation rates

The $^1H-^{15}N$ HSQC spectrum of the perdeuterated protease–DMP323 complex (Fig. 1) is relatively well resolved, even at 360 MHz, with significant resonance overlap only occurring for residues Leu[23], Asp[30], Ile[47], Ile[54], Ile[62], His[69], Ile[72], Gly[73], Thr[80], and Leu[97]. Relaxation measurements were carried out using pulse schemes described previously (Peng et al., 1991; Kay et al., 1992), with added pulsed field gradients for improved suppression of artifacts and of the water signal. $T_{1\rho}$ values were used instead of T_2 values because the latter can include errors of up to several percent as a result of resonance offset effects (N.

Tjandra and A. Bax, manuscript in preparation). The $T_{1\rho}$ relaxation times also depend on resonance offset, but this latter dependence is very straightforward (Davis et al., 1994):

$$1/T_{1\rho} = \cos^2\theta/T_2 + \sin^2\theta/T_1 \qquad (3)$$

where $\theta=\tan^{-1}(\Omega_N/\gamma_N B_1)$, Ω_N is the resonance offset and $\gamma_N B_1$ is the strength of the spin-lock field. Because T_1 and θ are known, T_2 can be calculated directly from the corresponding $T_{1\rho}$ and T_1 values. It is advantageous to keep θ as small as possible, i.e., to position the ^{15}N carrier at the midpoint of the spectral region of interest, and to use as high a B_1 value as possible without causing heating or other technical problems. In our study we have used a ^{15}N B_1 strength of 2.5 kHz at both fields. Amides whose resonance position relative to that of the solvent (lock) resonance is most sensitive to temperature (Lys[43], Asn[88], and Leu[89]) can be used as an indicator of the actual sample temperature. Such an analysis indicates that the increase in sample temperature resulting from even the longest ^{15}N spin-lock irradiation period is less than 0.1 °C. Relaxation times are shown graphically in Fig. 2.

Residues with internal motion

If proteins were rigid bodies, the diffusion tensor could be derived from the relation between T_1 or T_2 and the orientation of the N-H bond vector within the protein,
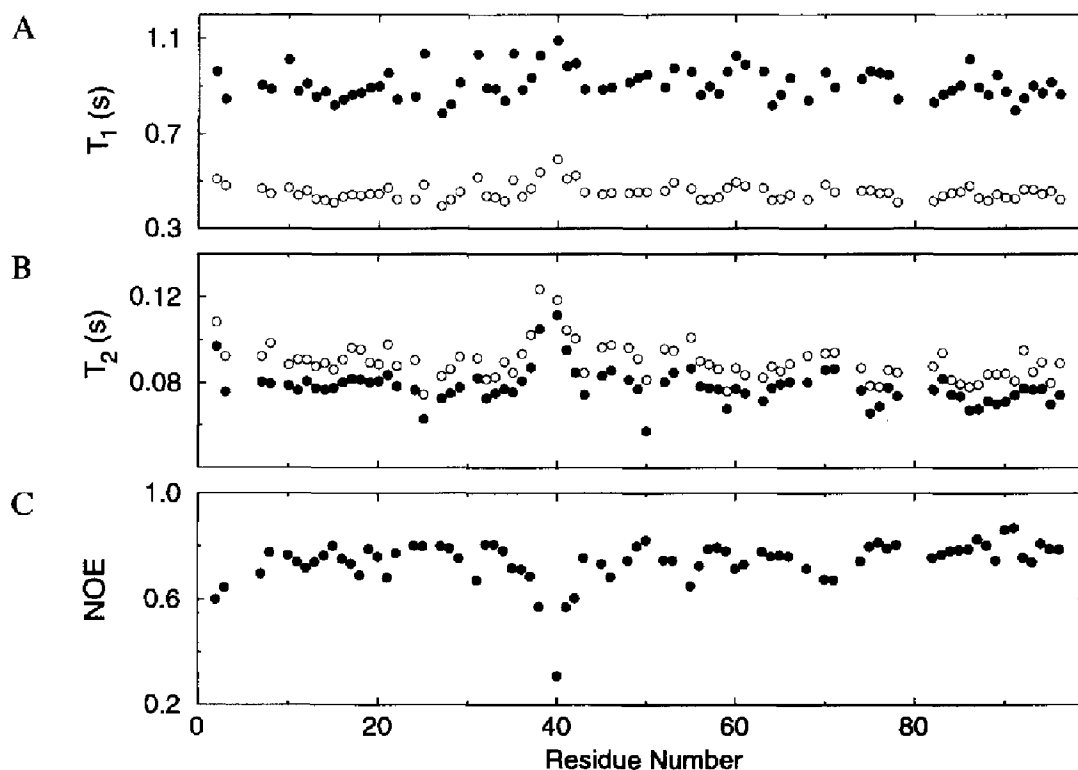

Fig. 2. Experimental values of (A) ^{15}N T_1 and (B) ^{15}N T_2, measured at 360 MHz (open circles) and 600 MHz (filled circles) ^1H resonance frequency, and (C) $^{15}N-\{^1H\}$ NOE values, measured at 600 MHz ^1H frequency.

TABLE 1
EXPERIMENTAL AND PREDICTED DIFFUSION PARAMETERS FOR HIV-1 PROTEASE COMPLEXED WITH DMP323[a]

Model	$\tau_{c,eff}$[b] (ns)	$2D_{zz}/(D_{xx}+D_{yy})$	D_{xx}/D_{yy}	θ[c] (°)	ϕ[c] (°)	ψ[c] (°)	E[d]	E_v
NMR (600)								
Isotropic	10.37[e]	1	1	–	–	–	457	7.19
	(10.58)[f]	(1)	(1)				474	(7.53)
Ax. symm.	10.65	1.34[e]	1	2.7[e]	176[e]	–	185	3.09
	(10.87)[f]	(1.34)	(1)	(2.8)	(177)		(191)	(3.19)
Constr. asymm.	10.59	1.35	1.11[e]	5.3	180	180	172	2.87
	(10.82)[f]	(1.37)	(1.11)		(180)	(180)	(177)	(2.96)
Asymm.	10.65	1.34	1.06	3.5	173	175[e]	168	2.90
	(10.87)[f]	(1.35)	(1.06)	(3.5)	(174)	(175)	(174)	(3.00)
NMR (360)								
Isotropic	10.58	1	1	–	–	–	305	4.92
	(10.71)[f]	(1)	(1)	–	–	–	(308)	(4.98)
Ax. symm.	10.88	1.40	1	3.6	177	–	116	1.96
	(11.00)[f]	(1.40)	(1)	(3.5)	(174)	–	(117)	(1.98)
Constr. asymm.	10.81	1.45	1.12	6.5	180	180	95	1.61
	(10.97)[f]	(1.44)	(1.11)	(5.7)	(180)	(180)	(94)	(1.59)
Asymm.	10.87	1.39	1.10	5.1	178	180	92	1.62
	(10.99)[f]	(1.40)	(1.10)	(5.1)	(178)	(180)	(93)	(1.63)
Hydrodyn. calc.[g]								
Asymm.	10.80	1.52	1.06[e]	5.5	163	175		

[a] At 27 °C, in water, for 2×64 residues, selected as described in the text.
[b] $\tau_{c,eff}$ is calculated from $[2Tr(D)]^{-1}$.
[c] Euler angles describing the orientation of the diffusion tensor in the principal axis frame of the inertia tensor.
[d] Using estimated random errors of 11 ms (600 MHz) and 6.8 ms (360 MHz) in T_1 and 2.3 ms in T_2 (both at 360 and 600 MHz).
[e] Rmsd values when repeating the calculation and randomly deleting 20% of the residues used in the fit are 0.02 ns ($\tau_{c,eff}$); 0.02 ($2D_{zz}/(D_{xx}+D_{yy})$); 0.01 (D_{xx}/D_{yy}); 0.2° (θ); 1° (ϕ,ψ).
[f] τ_c value obtained when subtracting 0.04 s^{-1} from experimental $1/T_1$ rates before fitting T_1/T_2.
[g] Using a bead model and half a shell of bound water.

using Eqs. 1 and 2b. The presence of very rapid internal motions causes nearly the same fractional increase in T_1 and T_2. Therefore, to a good approximation, the T_1/T_2 ratios are not influenced by such motions and can be used to derive the rotational diffusion tensor (Kay et al., 1989; Tjandra et al., 1995b). Special care needs to be taken so that residues with internal motions that are not extremely fast are excluded in such an analysis. Two separate cases can be distinguished. First, changes in $J(\omega_N)$ resulting from internal motions faster than the overall rotational diffusion but slower than ca. 100 ps can significantly alter the T_1 value, whereas the fractional change in T_2 is much smaller in the macromolecular limit. Residues with such internal motions also exhibit below-average NOE values, and all residues with a ^{15}N-{^1H} NOE smaller than 0.65 (measured at 600 MHz ^1H frequency) are excluded (Gln[2], Val[3], Leu[38], Gly[40], Arg[41], Trp[42]) when calculating the diffusion tensor from the T_1/T_2 ratios. Second, residues with conformational exchange occurring on a microsecond to millisecond time scale experience additional line broadening, commonly described by the exchange term R_{ex} (Clore et al., 1990a). In the present study, a residue n is excluded from the rotational diffusion analysis if the following criterion applies:

$$(\langle T_2 \rangle - T_{2,n})/\langle T_2 \rangle - (\langle T_1 \rangle - T_{1,n})/\langle T_1 \rangle > 1.5 \times SD \quad (4)$$

where the average is taken only over residues that have not been excluded because of a low NOE. In the above equation, $T_{1,n}$ and $T_{2,n}$ are the T_1 and T_2 values of residue n, and SD is the standard deviation calculated for these residues using the left-hand side of Eq. 4. Equation 4 is based on the fact that in the slow tumbling limit, rotational diffusion anisotropy results in equal but opposite fractional changes in T_1 and T_2. However, slow conformational exchange shortens T_2 but not T_1, causing residues with significant slow motion to fail Eq. 4. The R_{ex} contribution is largest at the highest field strength and the relaxation times measured at 600 MHz were used, resulting in the exclusion of residues Asp[25], Glu[35], Ile[50], Tyr[59], Val[75], Leu[76], and Gly[86]. In addition, residues Thr[4], Leu[5], Trp[6], Gly[51], and Asn[98] were excluded because of their vanishingly low intensity in the ^1H-^{15}N HSQC spectra, presumably also as a result of slow conformational exchange. Also excluding the six prolines, the previously mentioned 10 residues with overlapping ^{15}N-^1H correlations, six residues with low NOEs, and Ala[67], for which the N-H bond orientation is not known (Cys[67] in the X-ray structure), leaves 64 residues per monomer or 128 per dimer for which reliable T_1/T_2 ratios could be determined.

Since the exchange contribution to $1/T_2$ increases with the square of the magnetic field strength, an anomalously high ratio of the T_2 values measured at 360 and 600 MHz can be used instead of Eq. 4 as evidence for conformational exchange (Peng and Wagner, 1995; Phan et al., 1996). An exchange contribution that shortens T_2 by 1% at 360 MHz shortens it by nearly 3% at 600 MHz, increasing the $T_2(360)/T_2(600)$ ratio by ~2%. Based on the uncertainties in the T_2 values measured at 360 and 600 MHz (2.6 and 2.2%, respectively, see Materials and Methods), the random uncertainty in the ratio of the T_2 values measured at 360 and 600 MHz is 3.5%. The minimum experimentally detectable increase in $T_2(360)/T_2(600)$ (i.e, beyond 1.5 SDs) is therefore about 5%, which corresponds to a 7.5% exchange contribution at 600 MHz. Using the criterion of Eq. 4, one can identify exchange contributions at 600 MHz that are as small as 3.8%, owing in part to the low uncertainty (1.2%) in our experimental T_1 values. Therefore, in the present case Eq. 4 is used instead of the field dependence of T_2 for identifying residues subject to conformational averaging. If the T_2 ratio is used for identifying amides subject to exchange, only three residues are excluded and the rotational correlation time, diffusion anisotropy, and orientation of the diffusion tensor are the same (to within 0.1 ns, 0.01, and 2.2°, respectively) as the values obtained when using the criterion of Eq. 4. However, the residual normalized error in the fit is higher by 20% (data not shown).

Fitting the rotational diffusion tensor

The orientation and magnitudes of the principal com- ponents of the rotational diffusion tensor are searched to optimize the agreement between the observed T_1/T_2 ratios and ratios predicted using Eqs. 1 and 2b. For a monomeric protein, there are six unknown parameters: the principal components of the diffusion tensor, D_{xx}, D_{yy}, and D_{zz}; the polar coordinates θ and ϕ, describing the orientation of D_{zz}; and the angle ψ to define the orientation of D_{xx}, where $D_{zz} \geq D_{xx} \geq D_{yy}$. For a C_2-symmetric dimer such as HIV protease, one of the principal components of the diffusion tensor must align with the C_2 symmetry axis, and the number of unknowns is therefore reduced to four. As described previously (Tjandra et al., 1995b), the diffusion parameters are obtained by minimizing the difference, E, between the observed ('obs') and predicted ('pred') T_1/T_2 ratios:

$$E = \sum_n [(T_1^{obs}/T_2^{obs})^2 - (T_1^{pred}/T_2^{pred})^2] / \Delta^2 \qquad (5)$$

where Δ is the estimated error in the measured T_1/T_2 ratio, and the summation extends over all residues in the dimer for which reliable T_1 and T_2 values could be measured. The D_{xx}, D_{yy}, and D_{zz} components are uniquely defined by the apparent rotational correlation time, $\tau_c = [2 Tr(D)]^{-1}$, $D_\parallel/D_\perp$ (with $D_\perp = (D_{xx}+D_{yy})/2$ and $D_\parallel = D_{zz}$), and D_{xx}/D_{yy}. Table 1 shows the results obtained for these parameters when minimizing Eq. 5. First, the diffusion tensor is constrained to be isotropic, i.e., $D_{xx} = D_{yy} = D_{zz}$, and this one-parameter fit results in a high value of the error function, E. Second, the diffusion tensor is constrained to the axially symmetric model, i.e., $D_{xx}/D_{yy} = 1$, resulting in a significant reduction of the error function of this

TABLE 2
BEST FITS OF DIFFERENT DIFFUSION TENSORS TO EXPERIMENTAL AND RANDOMLY ASSIGNED 600 MHz DATA

	θ^a	ϕ^a	ψ^a	$\tau_{c,eff}^b$	$2D_{zz}/(D_{xx}+D_{yy})$	D_{xx}/D_{yy}	E	m^c
Isotropic	–	–	–	10.37			457	1
Ax. symm.								
I^d	2.7	176		10.65	1.34	–	185	4
II^d	45	60		10.37	1.08		427	4
III^d	67	178		10.38	1.06		429	4
IV^d	63	19		10.39	1.07		430	4
Constr. asymm.								
I^d	5.3	180	180	10.59	1.35	1.11	172	4
II^d	16.5	180	180	10.30	1.07	1.01	428	4
III^d	−16.5	180	180	10.28	1.09	1.04	437	4
IV^d	32.1	180	180	10.33	1.08	1.01	437	4
Asymm.								
I^d	3.5	173	175	10.65	1.34	1.06	168	6
II^d	58	150	157	10.39	1.09	1.01	424	6
III^d	32	156	122.7	10.39	1.03	1.07	424	6
IV^d	67	178	177	10.36	1.06	1.04	425	6

[a] Euler angles describing the orientation of the diffusion tensor in the inertia frame.
[b] Effective rotational correlation time, calculated from $(2TrD)^{-1}$.
[c] Number of variables used in the fit.
[d] Model I represents the experimental data set, where each T_1/T_2 ratio is correlated with the orientation of its N-H bond vector in the X-ray structure; models II–IV are the three sets (out of 20) that yield the lowest error function when T_1/T_2 ratios are randomly assigned to N-H vectors.
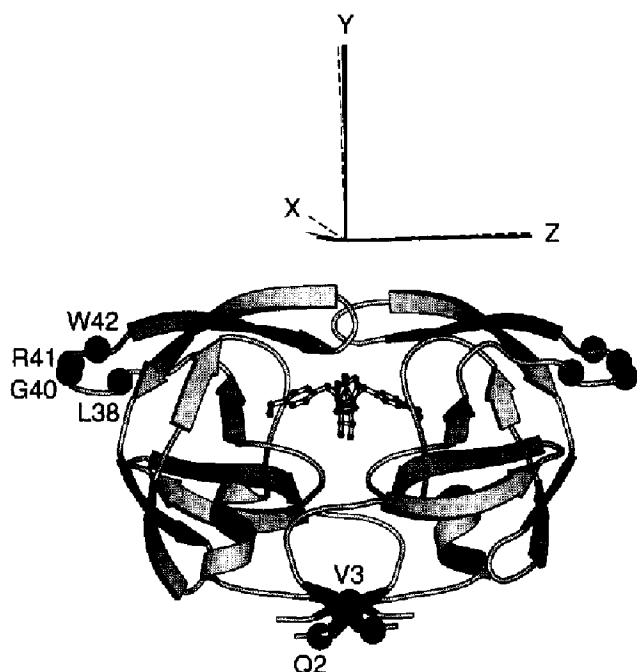
Fig. 3. Ribbon diagram of HIV-1 protease complexed with DMP323 (Lam et al., 1994). The solid, short-dashed, and long-dashed axis systems correspond to the principal axis orientations of the inertia tensor, the experimental diffusion tensor (600 MHz), and the diffusion tensor obtained from hydrodynamic modeling, respectively. Residues with NOE < 0.65 are marked in black.

four-parameter fit relative to the isotropic model. Note that the unique axis in the axially symmetric model is either collinear with or orthogonal to the C_2 symmetry axis of the complex. Fitting the data without any constraints imposed on the orientation of the axially symmetric diffusion tensor indicates that the unique axis is nearly orthogonal to the C_2 symmetry axis (Table 1). For the fully asymmetric model, the orientation of one of the principal axes of the diffusion tensor is fixed at the orientation of the C_2 symmetry axis. This four-parameter fit results in a further reduction of E. If the orientation of the diffusion tensor is not constrained (six-parameter fit), another small reduction in E is obtained. However, as will be discussed in more detail below, this latter reduction is a fitting artifact.

Statistical significance

The fit between a model and experimental data generally improves with the number of adjustable parameters in the model function. For this reason, one needs to evaluate whether the decrease in the error function obtained with an increase in the number of parameters is statistically significant. To this end, the so-called reduced error function is defined, $E_v(m) = E/(N-m)$, where N is the number of independently measured variables (here assumed to be equal to the number of residues, or 64), and m is the number of variables used in the fitting procedure (Bevington and Robinson, 1992). If two fitting procedures

with m and m+k variable parameters are performed, then the ratio of their E_v will follow an F distribution. In particular, a test for the validity of adding k additional terms can be carried out by calculating the following ratio:

$$F = [E(m) - E(m + k)] / [k E_v(m + k)] \qquad (6)$$

where E(m) is the result of fitting the data using (N−m) degrees of freedom (Eq. 5). A large F value justifies the inclusion of the additional terms in the fit. A more convenient measure is the normalized integral of the probability density distribution, P(F; k, N−m−k), which represents the probability that the observed improvement in the (m+k)-parameter fit over the m-parameter fit is obtained by chance. Typically, P values smaller than 0.01 are considered to be statistically significant. The normalization factor in Eq. 6, k, was erroneously omitted in Eq. 9 of Tjandra et al. (1995b). Use of the above test to evaluate the statistical significance of adding three degrees of freedom in the axially symmetric model (relative to the isotropic tumbling model) results in F = 29.3 at 600 MHz and F = 32.1 at 360 MHz. This corresponds to P(F,3,60) values smaller than 10^{-6}, both at 360 and 600 MHz.

A second test of the validity of the experimentally determined anisotropy can be carried out by randomly assigning the measured T_1/T_2 ratios to the 64 backbone amides in the protease homodimer. This removes the correlation between the orientation of the N-H bond vector and the measured T_1/T_2 ratio (Tjandra et al., 1995b, 1996a). The procedure was repeated 20 times, each time using a different set of random assignments. The results for the three fits that yielded the lowest value of the error function are listed in Table 2. As can be seen from this table, use of the axially symmetric model lowers the error function relative to the isotropic model, and use of the fully asymmetric diffusion tensor lowers it even further. However, the reduced error function remains significantly higher compared to the case where the correct N-H bond vector orientation is used for each T_1/T_2 ratio. This confirms that the use of an asymmetric diffusion tensor is statistically significant.

The decrease in E when removing the constraint imposed by the C_2 symmetry of the complex, which corresponds to an increase in the number of variables from four to six, is slightly larger for the 600 MHz data than for the data at 360 MHz (Table 1). However, as expected, for neither of the two data sets is there a reduction in E_v, indicating that the reduction in E is not statistically significant.

Hydrodynamic modeling

The hydrodynamic properties of the HIV protease dimer can also be predicted on the basis of its X-ray structure, using hydrodynamic modeling programs. Such programs typically calculate the hydrodynamic properties

using a bead replacement method (Garcia de la Torre and Bloomfield, 1981) in which the shape of the protein is approximated by a set of spherical beads. For a small protein such as ubiquitin, every non-hydrogen atom of the protein could be replaced by a sphere with a radius of 1 Å (Tjandra et al., 1995b), and excellent agreement between the diffusion tensors derived from NMR and from hydrodynamic modeling was found. For the considerably larger HIV protease, the bead replacement needed to be adapted to make the hydrodynamic calculations feasible. Details of the technical implementation of the hydrodynamic modeling procedure will be published elsewhere (S. Feller, R. Venable and R. Pastor, unpublished results). The results of these calculations are also summarized in Table 1, and again show good agreement with the NMR-derived rotational diffusion parameters. The orientation of the z-axis of the diffusion tensor from hydrodynamic modeling agrees to within 5° with the orientation of the experimentally obtained diffusion tensor. However, the anisotropy $2D_{zz}/(D_{xx} + D_{yy})$ obtained from hydrodynamic modeling is somewhat larger than the value obtained from the NMR relaxation data. This difference in the magnitude of the anisotropy may be caused by a higher-than-average degree of flexibility in the loops at the ex-

treme ends of the long axis of the protein (Fig. 3). For ubiquitin, it was found that in order to obtain good agreement between experimental and modeling diffusion tensors, the four highly flexible C-terminal residues needed to be deleted from the ubiquitin structure prior to calculating its hydrodynamic properties (Tjandra et al., 1995b). Analogously, it is conceivable that the experimentally observed flexibility at the extreme ends of the protease dimer, involving residues Leu[38]–Trp[42], is responsible for the smaller diffusion anisotropy. In the hydrodynamic calculations these regions were assumed to be rigid. The orientations of the z-axes of the experimentally derived and calculated diffusion tensors differ by less than 3° and are thus in excellent agreement with one another. Although the inertia and diffusion tensors represent different properties, and are not necessarily collinear, they have very similar orientations in the protease–DMP323 complex (Fig. 3, Table 1).

Analysis of internal motion

Using the rotational diffusion parameters listed in Table 1, it is straightforward to determine the values of S^2 and τ_e, using Eqs. 1 and 2b. The values are listed in the supplementary material and are shown graphically in Fig.
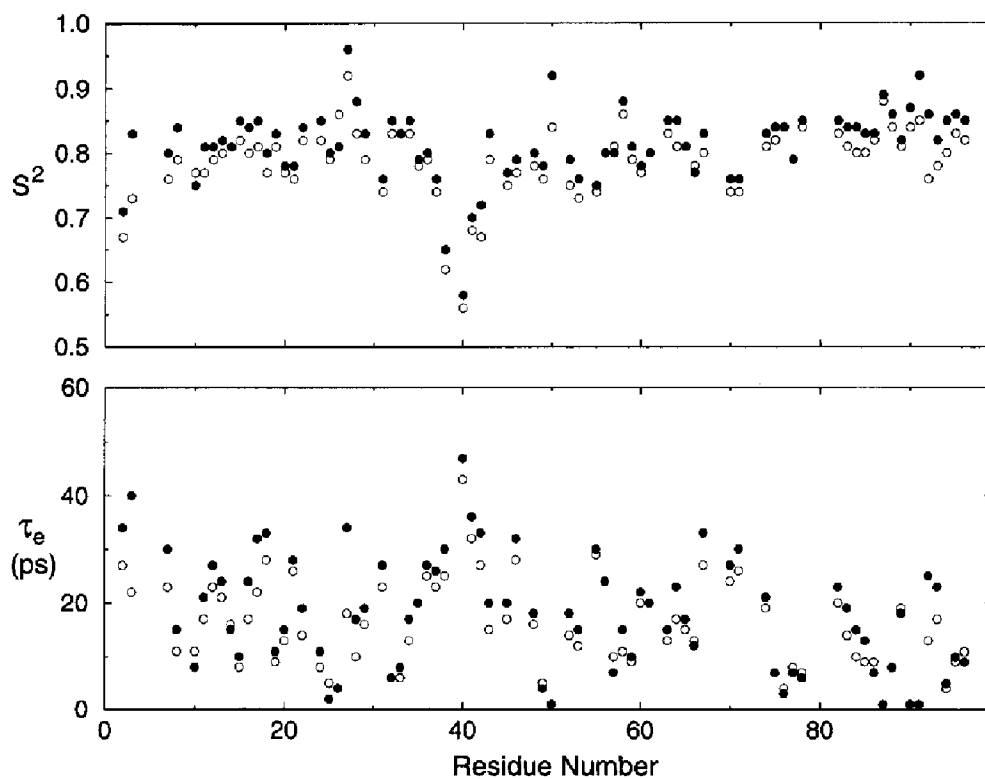

Fig. 4. Order parameters S^2 and internal correlation times τ_e obtained from 600 MHz (solid circles) and 360 MHz (open circles) data in the simple model-free formalism of Lipari and Szabo (1982). S^2 and τ_e values have been derived using an asymmetric diffusion tensor with a magnitude and orientation that are the average of the orientations and magnitudes of the diffusion tensor calculated from data at 360 and 600 MHz (Table 1). The effect of fast internal motions on the T_1/T_2 ratio is not accounted for, and the S^2 and τ_e values are based on a CSA value of 160 ppm. For residues Asp[25], Glu[35], Ile[50], Tyr[59], Val[75], Leu[76], and Gly[86], which have a significant exchange contribution, S^2 and τ_e values are calculated from T_1 and NOE data alone. For reasons of uniformity, residues with NOE < 0.65, for which the extended model-free approach typically gives a better fit to the experimental data, have also been treated with the simple model-free formalism.
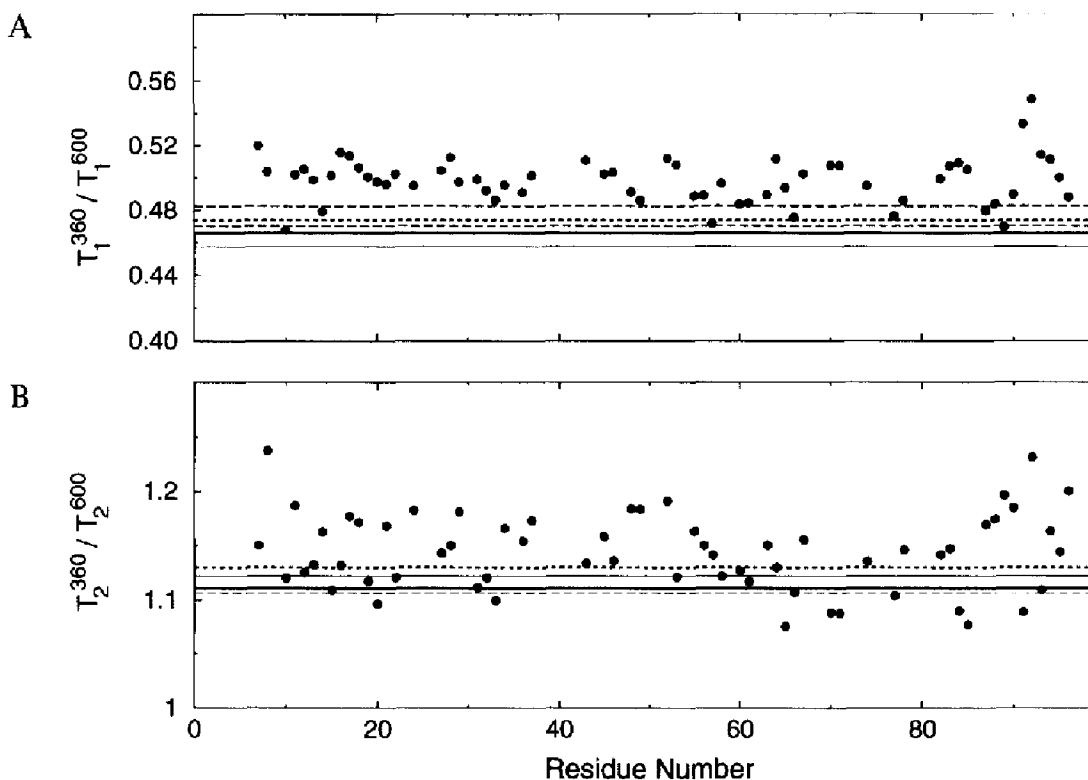
Fig. 5. Ratios of (A) T_1 and (B) T_2 values, measured at 600 and 360 MHz ^{1}H frequency in the HIV-1 protease–DMP323 complex for residues with NOE > 0.65, and not subject to slow conformational exchange. Thin solid and dashed lines correspond to the ratios expected for H-N vectors oriented parallel to the z-axis (long axis) and y-axis (short axis) of the diffusion tensor (Table 1), and with a ^{15}N CSA of 160 ppm. The heavy solid line corresponds to the ratio of relaxation times expected for a protein isotropically tumbling with $\tau_c = 10.7$ ns, CSA = 160 ppm, and no $1/T_1$ or $1/T_2$ contribution from internal motion; the heavy short dashed line is the ratio expected for $\tau_c = 10.7$ ns, CSA = 170 ppm, and no $1/T_1$ contribution from internal motion; the long-dashed heavy line is the ratio expected for $\tau_c = 10.7$ ns, CSA = 170 ppm, and a 0.04 s^{-1} $1/T_1$ frequency-independent contribution from rapid internal motion. The rapid internal motions have a negligible effect on the T_2 ratio and only the long-dashed heavy line is shown in (B).

4. As can be seen from this figure, there generally is a good agreement between the values of the order parameters derived from the relaxation data measured at 600 and 360 MHz, but values calculated from the 360 MHz data are systematically lower by $\sim 0.04 \pm 0.02$. Fitting both sets of data simultaneously results in values of the order parameter and τ_e that are intermediate between the two sets of values shown in Fig. 4. Note that the τ_e values are primarily determined by the T_1 and NOE data, and not by T_2, and contain considerable experimental uncertainty.

If S^2 and τ_e values are derived from the 600 MHz T_1, T_2, and NOE data using the assumption of isotropic rotational diffusion with $\tau_c = 10.4$ ns, instead of the diffusion tensor of Table 1, the order parameters remain similar to the values shown in Fig. 4 (pairwise rmsd 0.027); to a lesser extent this also applies for τ_e (pairwise rmsd 9 ps). This confirms calculations made by Schurr et al. (1994), which indicated that anisotropy of molecular reorientation has relatively little effect on order parameters derived from the combination of T_1, T_2 and NOE data. However, for many residues the fit of the relaxation data using the simple model-free spectral density equation of Lipari and

Szabo (1982a), which assumes isotropic tumbling and internal motion with one correlation time, τ_e, is unacceptably poor. In such cases one might be tempted to erroneously introduce an additional time constant for internal motion (if T_1/T_2 is too small) or an exchange term, R_{ex} (if T_1/T_2 is too large). Indeed, in the earlier study of the protease–DMP323 complex (Nicholson et al., 1995), residues Thr^{31}, Asp^{60}, Ile^{62}, and Thr^{80} were tentatively identified as being subject to slow conformational exchange, whereas in the present study it was found that their N-H bond vectors are oriented nearly parallel (within 30°) with the z-axis of the rotational diffusion tensor.

Field dependence of T_1 and T_2

As noted above, S^2 values derived from 360 MHz data are systematically lower than values derived from 600 MHz data by a statistically significant amount. Slightly larger systematic differences in S^2 are found when analyzing the 300 and 600 MHz relaxation data reported for eglin c (Peng and Wagner, 1995). As will be discussed below, this systematic difference is also reflected in the $T_1(360)/T_1(600)$ and $T_2(360)/T_2(600)$ ratios, which are higher than expected for a rigid rotor. We propose that

this discrepancy results from two separate causes: first, internal motions are not negligible when calculating the diffusion tensor from the T_1/T_2 ratios, and second, the CSA is, on average, about 10 ppm larger than the commonly used value of 160 ppm.

The experimental $T_1(360)/T_1(600)$ and $T_2(360)/T_2(600)$ ratios are shown in Fig. 5. Also indicated in this figure are the ratios expected for the case where internal motions are infinitely fast ($\tau_e = 0$). This latter ratio has a weak dependence on the rotational correlation time and, owing to the rotational diffusion anisotropy, predicted T_1 ratios fall in a narrow range between 0.458 and 0.470 and T_2 ratios are between 1.123 and 1.107 for N-H bond vectors parallel and perpendicular to the z-axis of the diffusion tensor of HIV protease. However, the assumption that $\tau_e = 0$ is clearly not valid. For example, a solid-state NMR study by Cole and Torchia (1991) of microcrystalline staphylococcal nuclease, selectively enriched with ^{15}N-Val and ^{15}N-His, indicates an average ^{15}N $1/T_1$ value of about 0.04 s^{-1}. This longitudinal relaxation is entirely caused by internal motions, as the overall motion of the protein is frozen in the crystalline state. Therefore, it is reasonable to assume that, on average, there will be a 0.04 s^{-1} contribution to the T_1 relaxation caused by internal motions. This contribution to the longitudinal relaxation rate results from internal fluctuations that are much faster than the ^{15}N Larmor frequency, and it is therefore

independent of magnetic field strength (neglecting the increase in the CSA term with higher field). This internal motion contribution to T_1 should be subtracted from the measured $1/T_1$ relaxation rates before the rotational correlation time is calculated from the T_1/T_2 ratios. Note that the finite time scale of the internal motions has a significant effect only on T_1 and not on the much shorter T_2.

If a uniform 0.04 s^{-1} contribution is subtracted from all measured $1/T_1$ values, calculation of the rotational diffusion tensor yields the same orientation and anisotropy for the diffusion tensor, but a decrease in the diffusion rate by ca. 2% at 600 MHz and 1% at 360 MHz (Table 2) relative to the values listed in Table 1. This results in an increase by 0.01 of the predicted $T_1(360)/T_1(600)$ ratio, thereby improving the agreement between the experimentally observed and predicted field dependence of T_1 (Fig. 5A). Nevertheless, on average, the experimentally observed ratio remains higher than predicted, and the rapid internal motions have a negligible effect on the $T_2(360)/T_2(600)$ ratios. These latter ratios are also higher than what is calculated for a rigid protein, assuming a ^{15}N CSA of 160 ppm and an internuclear ^{1}H-^{15}N distance of 1.02 Å.

The commonly used ^{15}N CSA value of 160 ppm is based on solid-state NMR studies of microcrystalline model peptides, carried out at or near room temperature (Oas et al., 1987; Hiyama et al., 1988). In the study by Hiyama et al., the strength of the ^{15}N-^{2}H dipolar interac-
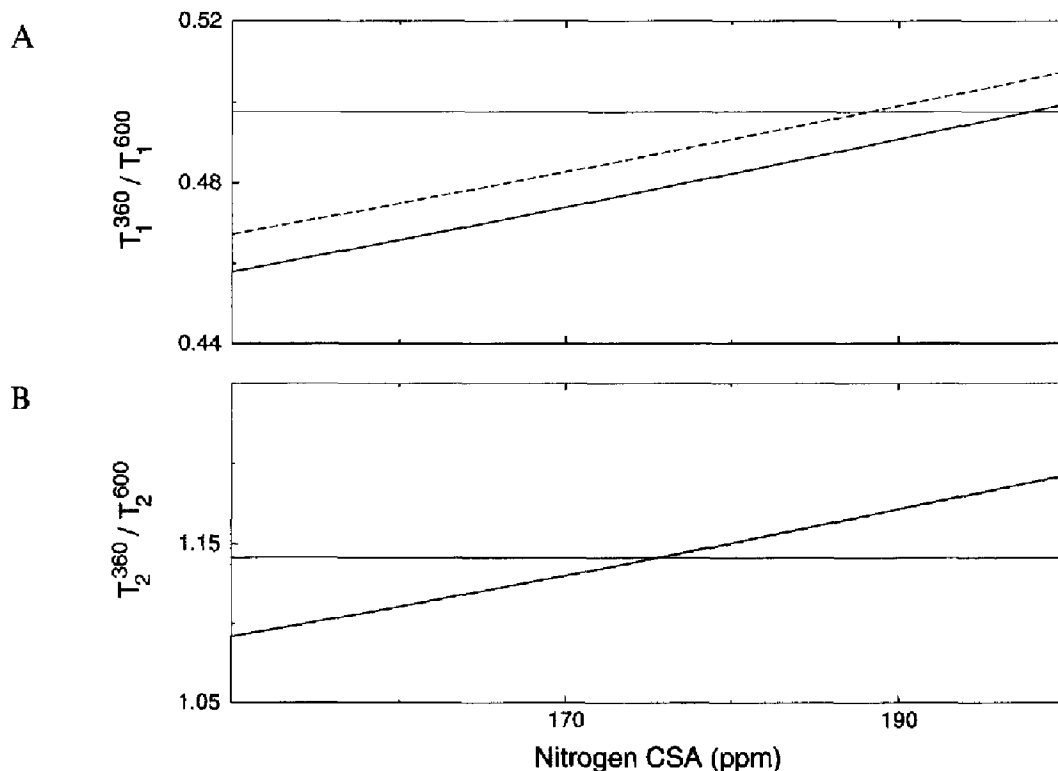

Fig. 6. Theoretical ratio of (A) T_1 values and (B) T_2 values measured at 600 and 360 MHz as a function of the magnitude of the ^{15}N CSA in the absence of internal motion (solid lines) and in the presence of a 0.04 s^{-1} $1/T_1$ contribution (dashed line) from rapid internal motion. Note that the rapid internal motion does not significantly affect the T_2 ratio, and the dashed line nearly coincides with the solid one in (B). Thin horizontal lines correspond to the experimentally observed average ratios for residues with NOE > 0.65, and are not subject to slow conformational exchange.

tion corresponds to an internuclear distance of 1.04–1.05 Å, which is about 7% weaker than the dipolar coupling expected for the commonly used ^{1}H–^{15}N distance of 1.02 Å. This difference was attributed to the effect of internal motions, which reduce the dipolar coupling by the order parameter S. The observed powder pattern width of 160 ppm is subject to the same degree of narrowing, and the static CSA powder pattern width is therefore expected to be ca. 7% larger, i.e., 170 instead of 160 ppm.

Shown in Fig. 6 are plots of the $T_1(360)/T_1(600)$ and $T_2(360)/T_2(600)$ ratios as a function of the ^{15}N CSA, expected for a protein tumbling isotropically with a τ_c of 10.7 ns, and a 0.04 s^{-1} $1/T_1$ contribution resulting from rapid internal motions. As can be seen from this figure, agreement with the experimentally observed ratios improves when the CSA value is increased from 160 to 170 ppm, but average CSA values of 175 ppm (T_2) and 187 ppm (T_1) would be needed to optimize the agreement. When using a CSA of 170 ppm and a 0.04 s^{-1} contribution to $1/T_1$ from internal motions, the average experimental $T_1(360)/T_1(600)$ and $T_2(360)/T_2(600)$ ratios each differ by less than 1 SD from their theoretical value. Nevertheless, the experimental $T_1(360)/T_1(600)$ and $T_2(360)/T_2(600)$ ratios both remain slightly higher than can be explained by theory. The possibility that this difference results from a small systematic error in the measurement cannot be excluded.

Use of a 170 ppm instead of a 160 ppm CSA value lowers the values of the generalized order parameter, S^2, by ca. 3.1 and 1.4% for the values derived from the 600 and 360 MHz relaxation data, respectively. Thus, the systematic discrepancy observed in Fig. 4 is largely removed and good agreement between the two sets of S^2 values is obtained, with a pairwise rmsd of only 0.026. The order parameters calculated in this manner are available as supplementary material. The difference in S^2 obtained from 360 and 600 MHz data is larger than 0.05 for only four residues, Val^3, Ile^{50}, Thr^{91} and Gln^{92}. For Val^3 and Ile^{50}, low NOE values suggest that the simple model-free approach is insufficient to describe the internal motions. For Thr^{91} and Gln^{92} it is not clear why the order parameters obtained from 360 and 600 MHz data are different.

It is interesting to consider how the predicted field dependencies of T_1, T_2 and S^2 change if the ^{1}H–^{15}N internuclear distance, r_{NH}, deviates from its estimated value of 1.02 Å. An increase in r_{NH} by 0.01 Å results in a 5.7% decrease of the constant d^2 in Eq. 1, and 5.4% (360 MHz) and 4.5% (600 MHz) increases in both T_1 and T_2. The resulting change in S^2, needed to fit the measured data, is an approximate increase by 5.4% (360 MHz) and 4.5% (600 MHz). This numerical example illustrates that the predicted field dependencies of T_1 and T_2 are only weakly influenced by the value of r_{NH}, and a deviation from $r_{NH} = 1.02$ Å cannot account for the systematic difference be-

tween S^2 values derived from 360 and 600 MHz data. Deviations much larger than 0.01 Å from $r_{NH} = 1.02$ Å yield unreasonable order parameters and therefore are not realistic.

Conclusions

NMR relaxation data indicate that the rotational diffusion tensor of HIV protease complex is asymmetric, and its orientation and magnitude are in good agreement with hydrodynamic modeling results. HIV protease is the first protein for which a statistically significant deviation from axially symmetric diffusion could be ascertained experimentally by NMR. The study was carried out on perdeuterated protease; the associated improved spectral resolution over protonated protease was particularly important for the data collected at 360 MHz. The data are in good agreement with those reported in a previous relaxation study, carried out at a slightly higher temperature (35 °C) on fully protonated protease complexed with the same inhibitor.

In the case of rotational anisotropy, T_1 and T_2 values deviate in opposite directions from their average value. As a result, order parameters derived from both the T_1 and T_2 data (plus the ^{15}N-{^{1}H} NOE) do not change much if the anisotropy of rotational diffusion is ignored during data analysis, although it may result in misidentification of an exchange contribution for residues with ^{15}N-^{1}H vectors parallel to the long axis of the protein. However, if, as has been suggested in the literature, J(0) (or T_2) is used as a marker for the order parameter, rotational anisotropy can result in a distorted picture of backbone mobility. The same applies to the case where the order parameter is obtained from the field dependence of the ^{15}N T_1 and the ^{15}N-{^{1}H} NOE (Schneider et al., 1992).

Analysis of the magnetic field dependence of the T_1 and T_2 relaxation times indicates that, contrary to a commonly used assumption, the effect of rapid internal motions on the T_1 relaxation rate, although small, is not negligible. The effect of these rapid internal motions has been estimated on the basis of a solid-state NMR study of a microcrystalline protein. Accounting for these internal motions increases the rotational correlation time derived from T_1/T_2 ratios by a few percent and decreases the field dependence of the ^{15}N T_1, but not T_2.

The field dependencies of ^{15}N T_1 and T_2 both suggest that, on average, the magnitude of the ^{15}N CSA is ca. 10 ppm larger than the commonly used value of 160 ppm, which was based on solid-state NMR studies in which the effect of rapid internal motions on the CSA powder pattern width was not taken into account. Recent quantitative measurements of relaxation interference between the ^{15}N-^{1}H dipolar interaction and the ^{15}N CSA also suggested an average CSA value larger than 160 ppm (Tjandra et al., 1996b).

284

Acknowledgements

We thank Attila Szabo and Dennis Torchia for many useful discussions, Frank Delaglio for software tools developed for optimal analysis of the experimental data, Rolf Tschudin for technical support, Dennis Torchia and Linda Nicholson for making the resonance assignments of the C67A mutant of the protease–DMP323 complex available to us, Richard Pastor, Scott Feller and Richard Venable for making available to us the results of hydrodynamic calculations prior to publication, Patrick Lam (Dupont-Merck) for providing the DMP323 inhibitor, Chong-Hwan Chang (Dupont-Merck) for providing us with the X-ray coordinates of the DMP323–protease complex, and James Ferretti (National Heart, Lung and Blood Institute) for use of the AMX-360 spectrometer. This work was supported by the Intramural AIDS Targeted Anti-Viral Program of the Office of the Director of the National Institutes of Health.

References

Allerhand, A., Doddrell, D., Glushko, V., Cochran, D.W., Wenkert, E., Lawson, P.J. and Gurd, F.N.R. (1971) *J. Am. Chem. Soc.*, 93, 544–546.

Barbato, G., Ikura, M., Kay, L.E., Pastor, R.W. and Bax, A. (1992) *Biochemistry*, 31, 5269–5278.

Bevington, P.R. and Robinson, D.K. (1992) *Data Reduction and Error Analysis for the Physical Sciences*, 2nd ed., McGraw-Hill, New York, NY, U.S.A., pp. 205–209.

Boyd, J., Hommel, U. and Campbell, I.D. (1990) *Chem. Phys. Lett.*, 175, 477–482.

Brüschweiler, R., Liao, X. and Wright, P.E. (1995) *Science*, 268, 886–889.

Clore, G.M., Driscoll, P.C., Wingfield, P.T. and Gronenborn, A.M. (1990a) *Biochemistry*, 29, 7387–7401.

Clore, G.M., Szabo, A., Bax, A., Kay, L.E., Driscoll, P.C. and Gronenborn, A.M. (1990b) *J. Am. Chem. Soc.*, 112, 4989–4991.

Cole, H.B.R. and Torchia, D.A. (1991) *Chem. Phys.*, 158, 271–281.

Davis, D.G., Perlman, M.E. and London, R.E. (1994) *J. Magn. Reson.*, B104, 266–275.

Dellwo, M.J. and Wand, A.J. (1989) *J. Am. Chem. Soc.*, 111, 4571–4578.

Garcia de la Torre, J. and Bloomfield, V.A. (1981) *Q. Rev. Biophys.*, 14, 81–139.

Grzesiek, S. and Bax, A. (1993) *J. Am. Chem. Soc.*, 115, 12593–12594.

Hansen, A.P., Petros, A.M., Meadows, R.P. and Fesik, S.W. (1994) *Biochemistry*, 33, 15418–15424.

Hiyama, Y., Niu, C.-H., Silverton, J.V., Bavoso, A. and Torchia, D.A. (1988) *J. Am. Chem. Soc.*, 101, 2378–2383.

Kay, L.E., Torchia, D.A. and Bax, A. (1989) *Biochemistry*, 28, 8972–8979.

Kay, L.E., Nicholson, L.K., Delaglio, F., Bax, A. and Torchia, D.A. (1992) *J. Magn. Reson.*, 97, 359–375.

King, R., Maas, R., Gassner, M., Nanda, R.K., Conover, W. and Jardetzky, O. (1978) *Biophys. J.*, 6, 103–117.

Kördel, J., Skelton, N.J., Akke, M., Palmer III, A.G. and Chazin, W.J. (1992) *Biochemistry*, 31, 4856–4866.

Lam, P.Y.S., Jadhav, P.K., Eyerman, C.J., Hodge, C.N., Ru, Y., Bacheler, L.T., Meek, J.L., Otto, M.J., Rayner, M.M., Wong, Y.N., Chang, C.-H., Weber, P.C., Jackson, D.A., Sharpe, T.R. and Erickson-Viitanen, S. (1994) *Science*, 263, 380–384.

Lipari, G. and Szabo, A. (1982a) *J. Am. Chem. Soc.*, 104, 4546–4558.

Lipari, G. and Szabo, A. (1982b) *J. Am. Chem. Soc.*, 104, 4559–4570.

London, R.E. (1980) In *Magnetic Resonance in Biology* (Ed., Cohen, J.S.), Wiley, New York, NY, U.S.A., pp. 1–69.

Nicholson, L.K., Yamazaki, T., Torchia, D.A., Grzesiek, S., Bax, A., Stahl, S.J., Kaufman, J.D., Wingfield, P.T., Lam, P.Y.S., Jadhav, P.K., Hodge, C.N., Domaille, P.J. and Chang, C.-H. (1995) *Nature Struct. Biol.*, 2, 274–280.

Nirmala, N.R. and Wagner, G. (1988) *J. Am. Chem. Soc.*, 110, 7557–7558.

Oas, T.G., Hartzell, C.J., Dahlquist, F.W. and Drobny, G.P. (1987) *J. Am. Chem. Soc.*, 109, 5962–5966.

Palmer III, A.G. (1993) *Curr. Opin. Biotechnol.*, 4, 385–391.

Peng, J.W., Thanabal, V. and Wagner, G. (1991) *J. Magn. Reson.*, 95, 421–427.

Peng, J.W. and Wagner, G. (1992) *Biochemistry*, 31, 8571–8586.

Peng, J.W. and Wagner, G. (1995) *Biochemistry*, 34, 16733–16752.

Phan, I., Boyd, J. and Campbell, I.D. (1996) *J. Biomol. NMR*, in press.

Schneider, D.M., Dellwo, M. and Wand, A.J. (1992) *Biochemistry*, 31, 3645–3652.

Schurr, J.M., Babcock, H.P. and Fujimoto, B.S. (1994) *J. Magn. Reson.*, B105, 211–224.

Torchia, D.A., Nicholson, L.K., Cole, H.B.R. and Kay, L.E. (1993) In *NMR of Proteins* (Eds., Clore, G.M. and Gronenborn, A.M.), MacMillan, London, U.K., pp. 190–219.

Tjandra, N., Kuboniwa, H., Ren, H. and Bax, A. (1995a) *Eur. J. Biochem.*, 230, 1014–1024.

Tjandra, N., Feller, S.E., Pastor, R.W. and Bax, A. (1995b) *J. Am. Chem. Soc.*, 117, 12562–12566.

Tjandra, N., Grzesiek, S. and Bax, A. (1996a) *J. Am. Chem. Soc.*, in press.

Tjandra, N., Szabo, A. and Bax, A. (1996b) *J. Am. Chem. Soc.*, in press.

Wagner, G. (1993) *Curr. Opin. Struct. Biol.*, 3, 748–754.

Woessner, D.E. (1962) *J. Chem. Phys.*, 3, 647–654.

Wüthrich, K. and Wagner, G. (1978) *Trends Biochem. Sci.*, 3, 227–230.